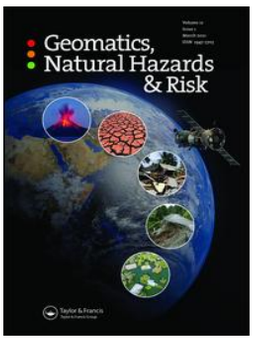

Geomatics, Natural Hazards and Risk

ISSN: (Print) (Online) Journal homepage: https://www.tandfonline.com/loi/tgnh20

Analysis of the spatiotemporal characteristics of drought disasters in North China during the Ming and Qing dynasties

Shuoben Bi , Shengjie Bi , Changchun Chen , Ying Lu , Athanase Nkunzimana & Yanping Li

To cite this article: Shuoben Bi , Shengjie Bi , Changchun Chen , Ying Lu , Athanase Nkunzimana & Yanping Li (2020) Analysis of the spatiotemporal characteristics of drought disasters in North China during the Ming and Qing dynasties, Geomatics, Natural Hazards and Risk, 11:1, 2509-2539, DOI: 10.1080/19475705.2020.1848929

To link to this article: https://doi.org/10.1080/19475705.2020.1848929

© 2020 The Author(s). Published by Informa UK Limited, trading as Taylor & Francis Group.

Published online: 25 Nov 2020.

Submit your article to this journal

Article views: 158

View related articles

View Crossmark data

Full Terms & Conditions of access and use can be found at
https://www.tandfonline.com/action/journalInformation?journalCode=tgnh20

GEOMATICS, NATURAL HAZARDS AND RISK
2020, VOL. 11, NO. 1, 2509–2539
https://doi.org/10.1080/19475705.2020.1848929

Taylor & Francis
Taylor & Francis Group

OPEN ACCESS Check for updates

Analysis of the spatiotemporal characteristics of drought disasters in North China during the Ming and Qing dynasties

Shuoben Bi[a], Shengjie Bi[b], Changchun Chen[a], Ying Lu[a], Athanase Nkunzimana[a] and Yanping Li[a]

[a]School of Geographical Sciences, Nanjing University of Information Science and Technology, Nanjing, China; [b]Department of Computer Science, Dartmouth College, Hanover, NH

ABSTRACT

The present study sought to understand the spatiotemporal characteristics, associated with changes in drought disasters during the Ming and Qing Dynasties in North China. The grade sequence of drought disasters at 21 sites for the given period (1470–1912 AD) in North China was studied herein. An ensemble empirical mode decomposition (EEMD) was used to analyze the multiple time-scales towards generating a simple and stable intrinsic modal function component. Comparisons and analysis of the frequency and intensity of drought disasters were made using polynomial fitting curves to understand the temporal variations of drought disasters. Two aspects were explored to study the spatial distribution and characteristics of drought disasters. The reconstruction of the sequence of drought disasters was based on the Empirical Orthogonal Function (EOF) and Rotated Empiric Orthogonal Function (REOF). The drought disaster was divided into several space modes and sensitive areas. Drought frequency was recurrent in the northern and low in the southern part of North China. Findings revealed drought frequency and intensity were high in southeast and low in the southwestern part of North China. The study would inform decisions on disaster prevention and mitigation thereby serving as a baseline print for predicting modern drought disasters.

ARTICLE HISTORY
Received 18 April 2019
Accepted 5 November 2020

KEYWORDS
Drought disaster; EEMD; EOF; REOF; spatiotemporal characteristics

1. Introduction

Drought is one of the challenging and widely distributed natural phenomena, which may last for weeks, months, years or even decades (Gaire et al. 2019). The dynamic variations in temperature and precipitation have altered the intensity and frequency of drought hazards, which pose potential threats on water resources, agriculture production and the overall health of ecosystems (Devkota et al. 2017; Katsanos et al. 2018). Studies

CONTACT Shuoben Bi bishuoben@163.com

© 2020 The Author(s). Published by Informa UK Limited, trading as Taylor & Francis Group.
This is an Open Access article distributed under the terms of the Creative Commons Attribution License (http://creativecommons.org/licenses/by/4.0/), which permits unrestricted use, distribution, and reproduction in any medium, provided the original work is properly cited.

revealed global warming-induced by climate change might intensify the occurrence, magnitude and duration of droughts in future with more devastating impacts (Piao et al. 2017). Generally, droughts can be classified into four (4) main types constituting meteorological droughts caused by inadequate precipitation in climatology over a particular geographical area (usually takes a lengthy period); agricultural droughts caused by insufficient soil moisture and crop water balance; hydrological droughts, on the other hand, are caused by river flow or water levels, canals or reservoirs falling below established statistical average or threshold (Dracup et al. 1980). Socio-economic droughts emanate from the aforementioned types of drought on the supply and claim of economic goods and services (Wilhite and Glantz 1985). Capability to show the spatial distribution of drought conditions and characteristics on different time scales is another important feature that this study sought to achieve. Global warming is exacerbating the severity of droughts at the local, regional, national and continental scale. The significance of drought studies is essential mainly as a result of the adverse effects of this natural phenomenon based on evidence of current and existing literature on climate sensitive crops, livelihoods and the environment (Zou et al. 2005; Lin et al. 2013). Zou et al. (2005) in their study revealed severe droughts in North-China affected several agricultural areas thereby causing an estimated loss of about 40 million hectares. They further reiterated that dry climatic conditions were accompanied by droughts, dust-storms, water scarcity and desertification across its localities or regions. These conditions affected several livelihoods and productivity, hence, becoming a major concern for the central government and the general public. Historically, agricultural civilization began in North China along the lower reaches of the Yellow River (Li and Lin 1993; Zou et al. 2005). Despite the major shift of economic activities from the north to the southern part of China, North China is highly characterized by agricultural and other economic activities. The influx of dry conditions in the region over the years has significantly affected the direct and indirect benefits of socio-economic events in arid and semi-arid areas. More so, drought studies in North China have increased awareness, aimed at providing a comprehensive overview of drought events linked to geo-hazards along with diverse and costly impacts, mitigation measures and so on. The present study is expected to analyze the spatiotemporal characteristics, associated with changes in drought hazards during the Ming and Qing dynasties in North China.

Apparently, several scholars have researched drought disasters in North China. Zhou (2009) analyzed the inter-annual summer variation of rainfall using modern platform precipitation data and explained the relation between the precipitation in North China, Northwest China and the Middle Yangtze River region. Ma et al. (2007) analyzed the characteristics of dry and wet change in North China from 1951 AD to 2005 AD. He identified that nearly 55 years experienced wet to dry processes, the turning point occurred in the mid and late 1970s. Rong et al. (2008) used statistics on the distribution rate of droughts from 1997 AD to 2002 AD and discovered that the persistent drought in North China is as a result of the interaction between the sub-members of the scale circulation system in the Eurasian region. Li et al. (2002) proposed a new calculation model scheme for the dry and wet index, analyzed the characteristics of the linear index variation of the drought in North China in the last half-century. They indicated an intense change in the drought potential in North

China and used singular spectrum analysis to test the periodicity of the time series. Zhou et al. (2014) used the standardized precipitation index of evapotranspiration and analyzed the spatiotemporal distribution of the drought intensity in North China. Gao and Zou (2013) identified the collation and analyzed the history of the Ming Fen River Basin drought using the county as a drought grade division standard. They used the linear trend estimation method to estimate the spatiotemporal changes of drought conditions of the Fen River Basin. They further employed two aspects of the frequency and intensity models to study the spatial distribution of drought along with the t-test to ascertain the change in drought dynamics with time.

Lu et al. (2016) used the methods of standardized precipitation evapotranspiration index (SPEI), M-K trend analysis, wavelet analysis among others to analyze the inter-annual change trend of drought, the change characteristics of drought frequency, dynamics in dry and wet cycle, trend variations in the four seasons, and the fluctuations in drought frequency over the North China Plain. Analysis of these parameters revealed the spatiotemporal characteristics of droughts over the North China Plain. Liu et al. (2013) analyzed the characteristics of inter-annual and inter-decadal extreme droughts and climatic factors according to the meteorological data during 1962—2011 AD from 35 meteorological stations in the North China Plain by using inverse distance weighted interpolation, M-K mutation testing, and linear trend estimation. Liu et al. (2015) provided a comprehensive analysis of the spatial and temporal variations of drought and its influencing factors in the North China Plain from 1960 to 2013 AD using the Palmer drought index (PDSI), empirical orthogonal decomposition (EOF), trend analysis, and correlation analysis. Based on the monthly precipitation data for 1960–2008 period, the spatial characteristics of drought hazards in China were investigated using a GIS-based drought hazard assessment model by He et al. (2011). Their findings suggested that the spatial distribution of drought hazard in China shows an apparent east-west difference, with the eastern part of China being far more susceptible than the western part. Yi et al. (2012) reported an attempt of quantitative climate reconstruction covering the main part of north-central China, by combining historical drought/flood index and tree-ring data.

Trend analysis, wavelet analysis and empirical orthogonal function were also applied to investigate changing trends, periodic and regional characteristics respectively. Zuo et al. (2018) used the non-parametric Mann-Kendall test to explore the temporal trends of precipitation, air temperature, and the SPEI drought index using data from 23 meteorological stations in Shandong Province in Eastern China.Chen et al. (2019) in their study analyzed the spatial and temporal variability of dryness/wetness based on data obtained from 75 meteorological stations in the middle and lower reaches of the Yangtze River Basin for 1960–2015 period. Spatiotemporal patterns of drought from 1961 to 2013 over the Beijing-Tianjin-Hebei (BTH) region of China were analyzed using PDSI based on data from 21 meteorological stations (Zhang et al. 2019). The EOF method was adopted to characterize drought patterns. Using historical meteorological data and other parameters, Wang et al. (2020) analyzed drought characteristics in northern Shaanxi of China during the historical period (1960–2018) and the future (2020–2100). Analysis was done using detrending procedure, Mann–Kendall's trend test (MK), EOF spatial analysis, and wavelet

analysis. Using Mann-Kendall's trend test, the continuous wavelet transform (CWT), the rotated empirical orthogonal function (REOF), and the random forest method (RF), the study focused on the trends and spatial variability in wetness/dryness. Several studies have revealed the potential factors influencing droughts by analyzing the behaviour of precipitation in Southwest China (Rong 2004; Wang et al. 2020). Moreover, Hao et al. (2020) and An et al. (2014) investigated the characteristics of temperature variations on decadal–centennial scales during 950–1250 AD era for four (4) regions constituting Northeast, Northwest, Central-east, and Tibetan Plateau in China, using historical documents. The ensemble empirical mode decomposition method was used to analyze the time series.

Contextually, North China lies within the arid and semi-arid zone. In recent decades, drought occurrence is common in North China, hence, attracting extensive attention coupled with heightened concerns from experts and scholars. The 'China Science and Technology of the Blue Book No. 5' classified drought as a major climate disaster in China. Existing literature shows drought intensity and frequency in North China is the highest across the country (Li and Qin 2013). The existence of some differences in geographical significance, transitional boundaries and meteorological divisions in North China cannot be overlooked. We selected the following four (4) provinces and two (2) municipalities respectively, thus, Hebei, Shanxi, Shandong, Henan, Beijing and Tianjin as the study area. The study region lies between 31°N–43°N and 110°E–123°E (as depicted Figure 1). Presently, there is a paucity of information on the characteristics of drought disasters in North China tracing back to historical periods during the Ming and Qing dynasties. Therefore, it is of great significance to bridge this knowledge gap to enhance the understanding of the frequency and development of drought disasters in the near future, coupled with drought prevention and control mechanisms. Despite the existence of measurable data as well as literature on droughts in North China, there is still considerable knowledge gap on using the spatial distribution of drought disasters and climate statistical methods to analyze the spatial characteristics of drought disasters. The present study focused on previous studies with reference to time and evolution of drought disasters. This paper dwelt on historical records of drought disasters in North China during the Ming and Qing Dynasties.

The main research contents and methods of the paper are shown as a flowchart in Figure 2.

2. Data and methods

2.1. Data sources

The important resources in this paper were mainly obtained from 'The chronology of drought in North China over the past five hundred (500) years' (Central Weather Bureau in North China 1975; Zhang 2009) (referred to as 'Drought chronology'), this historical drought and flood data were compiled by Zhang (2004) based on the 'China meteorological records collections of three thousand years' (referred to as 'General collection'). The historical data in this paper covered a total of 443 years, from 1470 AD to 1912 AD, from the mid-Ming Dynasty to the late Qing Dynasty. The historical data from 1470 AD (early Ming Dynasty) was relatively scattered, which hindered the

Figure 1. The location of North China in P. R. China.

separation of serial data; hence, it could not be put in sequence. 21 representative stations were selected to achieve the overall objectives for this study (Figure 3).

The 'Drought chronology' characterizes grade of drought disasters in North China (Zhang 2009). Classification and limitations of general drought in the 21 representative stations constitute Beijing–0 records, Tianjing–10 records, Hebei Province (Tangshan–0 records, Cangzhou–10 records, Baoding–0 records, Shijiazhuang–0 records, and Handan–0 records), Shandong Province (Jinan–0 records, Dezhou–0 records, Yantai–22 records, Heze–0 records, and Linyi–0 records), Henan Province (Anyang–33 records, Zhengzhou–0 records, Luoyang–61 records, Nanyang–183 records, and Xinyang–117 records), and Shanxi Province (Datong–14 records, Taiyuan–0 records, Linfen–0 records, and Changzhi–30 records). Searching the 'Historical drought and flood data', if the level of one year is 4 (slight drought), and it does not exist in the 'Drought chronology,' the given year is characterized as grade 1 (general drought). We obtained three types of data. The first type was the drought disaster rank sequence for the 21 sites from the Ming and Qing Dynasties (1470 − 1912 AD) in North China. The second type of data was the drought county number sequence for each city in each year during the Ming and Qing Dynasties in North China. The third type was the drought duration sequence in each year during the Ming and Qing Dynasties in North China.

In contrast to the 'General collection' and 'Historical drought and flood data', one year of disaster records is missing in the 'Drought Chronology'. If the data were not recorded in all three reports, the drought was considered as not having occurred in the

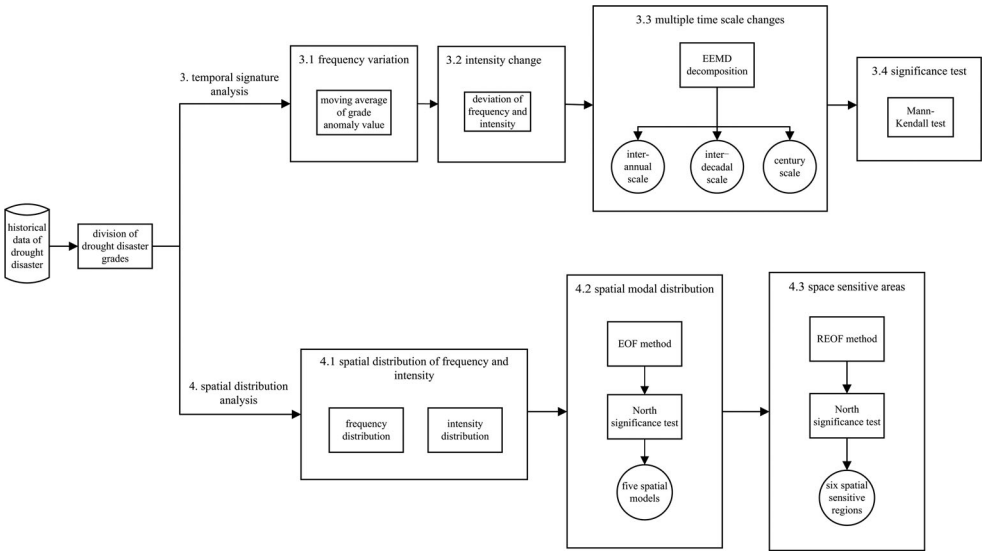

Figure 2. The flow chart of research framework.

region. This paper used the data with respect to three sources of information to determine the rank sequence of droughts at 21 sites during the Ming and Qing Dynasties era from 1470 AD to 1912 AD. The criteria for the classification of disaster grades are listed in Table 1. Level 1 was set as 'general disaster', level 2 on the other hand representing 'high drought', level 3 reflecting 'heavy drought', and 'no drought' set as level 0.

2.2. Temporal analysis methods

2.2.1. Ensemble empirical mode decomposition (EEMD)

Ensemble Empirical Mode Decomposition (EEMD) (Huang and Wu 2008) is an adaptive technique of analyzing time series considering both time and space. The method was developed recently and is widely used due to its suitability in analyzing nonlinear and non-stationary time series. The core idea of EEMD is to assemble the Gaussian white noise in the original signal into a hybrid sequence. This, in essence, ensures continuity of new signals at different time scales. In addition, the signal characteristics of extreme points are changed (Xue 2007). Similarly, the intrinsic mode function (IMF) satisfies two conditions (Sun et al. 2012), thus; i) over the entire period, the local extrema of each component (IMF) are equal or at most differing by one from its zero crossings, and ii) at one point, the average between the envelope of local maxima and local minimum must be 0 (Peel et al. 2011; Sun and Lu 2013; Xue et al. 2013). White noise $n_i(t)$ is added to the original signal x(t), hence:

$$x_i(t) = x(t) + n_i(t) \tag{1}$$

where $x_i(t)$ is the signal with added white noise after i times (Sun et al. 2012). Then, the IMF component is obtained by EEMD decomposition $C_{ij}(t)$. To eliminate the influence of artificial white noise, the average sum of the IMF components obtained by EEMD decomposition for N times is taken as the final IMF component, expressed as:

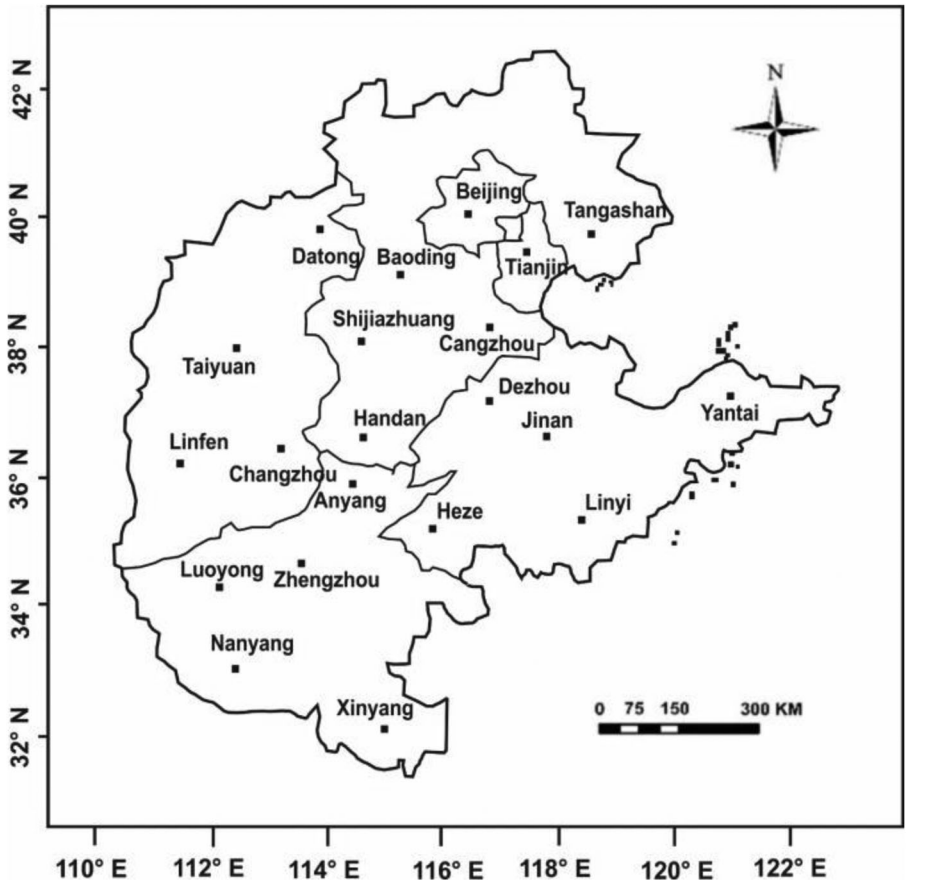

Figure 3. The data sites in North China.

$$C_j(t) = \frac{1}{N}\sum_{i=1}^{N} C_{ij}(t) \tag{2}$$

where $C_j(t)$ represents the j component obtained after the EEMD decomposition of the original signal. The influence of white noise on the analysis of signals follow the following statistical law:

$$e = a/\sqrt{N} \tag{3}$$

where e connotes the standard deviation (the deviation between the input signal and the reconstructed result of the corresponding IMF component). The symbol, a, represents the magnitude of the Gaussian white noise. It can be seen that when the noise margin remains the same, with a greater total number, the closer the final decomposition result is to the true value. Regarding the amplitude of the added noise, if the amplitude is small and the signal-to-noise ratio is too high, the noise will not affect the selection of the pole, which eventually results in losing its role on a supplementary scale. In general, $e = 0.2$ and $N = 100$ (Zhu et al. 2013). Finally, the original signal $x(t)$ can be decomposed into:

Table 1. Repartition of the standard grade classification of drought disasters.

Description of historical data for disasters	Drought disaster grade
'Spring drought', 'summer drought', 'winter and spring without rain'	1
'Summer and autumn high drought', 'spring and summer high drought', 'since the last year's winter solstice high drought, this year it started raining in July', 'for several months without rain as dry grain'	2
'Scene of utter desolation', 'tragic story of ancients driven by hunger to eat the flesh of each other's son', 'year after year of drought', etc.	3

$$x(t) = \sum_{j=1}^{n} c_j(t) + r_n(t) \tag{4}$$

where $r_n(t)$ is a trend item (*RES*), representing the general trend of the signals. Each component ($c_1(t)$, $c_2(t)$, … , $c_n(t)$) represents the fluctuations of the original signal at different time scales, with oscillating periods from small to large. At the same time, EEMD can also be used to conduct a significance test given the reliability of each IMF component.

2.2.2. Mann-Kendall (M-K)

The M-K test method is a nonparametric statistical test method widely used by climatologists and statisticians to test the variations of trends in a sequence. It is used to identify mutation points existing in the sequence and does not require samples to conform to a particular distribution, unperturbed by a smaller number of outliers (Wei 1999). The test process has been outlined in the mathematical expression (Equation 5) below.

For one time sequence, x_1, x_2, … , x_n, s_k represents the cumulative number ($x_i > x_j$-$1 \le j \le i$). A definition of statistics or parameter is given under the assumption that the time series is stochastically independent:

$$UF_k = \frac{[s_k - E(s_k)]}{\sqrt{Var(s_k)}} \quad k = 1, 2, ..., n \tag{5}$$

where UF_1=0, $E(s_k)$ and $Var(s_k)$ are the mean and variance of the cumulative number (s_k), respectively. Calculated as:

$$E(s_k) = n(n+1)/4 \tag{6}$$

$$Var(s_k) = n(n-1)(2n+5)/72 \tag{7}$$

Given the significance level in relation to the normal distribution table, if $|UF_i| > U\alpha$, there will be a marked trend change in the sequence. Based on the inverted sequence of the time series (x_n, x_{n-1}, … , x_1), the above process is repeated (UB_k=-UF_k, $k = n$, n-1, … , 1, UB_1=0). Graphs of UF_k and UB_k are drawn. The point of intersection is the point where mutation begins between the critical lines. The M-K test has the advantage of adhering to simple calculations, clearly defining the time at which the mutation started. Additionally, it points out the mutant region (Chen et al. 2011; Zhang et al. 2013; 2015).

2.3. Spatial analysis methods

The EOF (Wu 2005), also known as PCA, is commonly used to structurally characterize matrix data along with the extraction of data features. It can decompose and process irregular meteorological elements within the field into time coefficient and space vector features. The spatial modes must to some extent reflect the spatial distribution of meteorological elements. The transformation of REOF is based on the EOF decomposition, orthogonal rotation of the original matrix (maximum variance rotation), and high load vectors concentrated in a few variables. The remaining region is close to 0, which explains that the characteristics of field elements in rotation are more stable, clearer and more prominent over time prominent (Chen et al. 2010; Han et al. 2014; Liu et al. 2014; Liu and Xu 2014; Wang and Yan 2014).

2.3.1. Empirical orthogonal function (EOF) decomposition

EOF decomposition technology has the following prominent features (Wei 1999): (1) no fixed function, unlike some decompositions that rely on a special function; (2) Decomposition of irregular distribution of meteorological elements coupled with mutual orthogonality between the space vector features; the spatial mode reflects the spatial distribution characteristics of the elements. The time coefficient reflects the weight change of the corresponding spatial mode with time; (3) faster convergence rate with information on variable field dwelling on first few modes, and (4) the spatial structure of the separation has some specific physical attributes or meanings.

The primary coverage of the EOF analysis method follows Wei's analysis (1999). The observation data of a climate variable field in the form of a matrix is expressed as:

$$X = \begin{pmatrix} x_{11} & x_{12} & \cdots & x_{1n} \\ x_{21} & x_{22} & \cdots & x_{2n} \\ & \cdots & \cdots & \\ x_{m1} & x_{m2} & \cdots & x_{mn} \end{pmatrix} \tag{8}$$

where m is the mean spatial point and n is the mean time series length.

The natural orthogonal expansion of the meteorological time series means that X is decomposed into two parts, thus, the time function Z and the spatial function V:

$$X = VZ \tag{9}$$

or

$$x_{it} = \sum_{k=1}^{p} v_{ik} z_{kt} = v_{i1} z_{1t} + v_{i2} z_{2t} + \cdots + v_{ip} z_{pt} \tag{10}$$

where $i = 1,2, \ldots, m, t = 1,2, \ldots, n, k = 1,2, \ldots, p$

In the expression above, the t climatic observations on the i-th grid point can be seen as a linear combination of v_{ik} (the amount is p) and the time function z_{kt}.

At present, EOF as a basic analytical tool is commonly used in the field of atmospheric sciences (Shen et al. 2012; Chen et al. 2013; Yang et al. 2013).

2.3.2. Rotated empirical orthogonal function (REOF) decomposition

The REOFdecomposition is based on the EOF decomposition. The orthogonal rotation of the original matrix results in a high load vector concentrated in a small number of variables, with the load values of the other regions close to 0. The characteristic field obtained after rotation becomes more stable in the temporal dimension, and the spatial distribution structure becomes clearer, which can highlight and reflect local characteristics along with changes of each region (Ding et al. 2007; Liu and Ye 2007; Chen et al. 2010). The first several eigenvectors of the EOF expansion can maximize the variability structure of the whole region of the climate variable field. However, the separated spatial distribution structure cannot clearly express the characteristics of different geographical regions. By using the REOF analysis, we can overcome the error caused by the inconsistency in the region and temporal sampling in the EOF analysis. If the EOF analysis intercepts the first K spatial patterns and the cumulative total variance has reached a certain value (such as 80%), the K spatial type can be adjusted again, so that the percentage of the total variance of the adjusted K spatial pattern is unchanged. Contrarily, the single spatial model can reflect the local correlation results. In a scenario where the variance of the V component is significant, the T component has a variance maximum in the principal component (Han et al. 2014; Liu et al. 2014; Liu and Xu 2014; Wang and Yan 2014).

2.3.3. The differences between EOF and REOF

The basic principle of EOF is to decompose the field with P spatial points with time as a function. The first eigenvector of EOF expansion seeks to maximize the variability of the entire climatic region (Wei 1999). REOF analysis relies on the EOF to do the rotational changes. It enables the space field and the main components of the high value of the region to be concentrated in a smaller range making it easier to identify a spatial type. Surprisingly, not only can it reflect the changes in different regions, but can also reflect the distribution of different regions. The modal is noted as a load vector rotation factor (Wu and Huang 2015).

EOF and REOF analysis are statistical analysis methods designed to analyze the temporal and spatial variation characteristics of meteorological elements in a region due to its ability to simplify the original eigenvector structure and reflect climatic features (Tang et al. 2011). Here, more emphasis is placed on the overall correlation structure of the entire field with limited emphasis on the local correlation structure. This is eventually not conducive for the identification of elements distribution. Nevertheless, the REOF analysis can better highlight the local characteristics of the abnormal distribution of elements (Chen et al. 2010).

2.4. Spatial modal distribution of drought disaster

The EOF and REOF are specifically useful for the extraction of meteorological data; they can reflect the spatial distribution of meteorological data (Li et al. 2000). Therefore, EOF and REOF are used in this paper to explore the degree of the spatio-temporal evolution of drought disasters during the Ming and Qing Dynasties in North China. We focused on the analysis of spatial distribution and provided the

distribution level of drought disasters in North China coupled with a basic partition prediction. The EOF method was used for the classification of drought disaster rates, aimed at resolving the standard anomalies of the 21 selected sites in North China during the 443 years during the Ming and Qing Dynasties to generate the space load vectors. The first '*i*' vector features for the '*x*' field contribution rate are

$$\rho_i = \lambda_i / \sum_{i=1}^{m} \lambda_i \tag{11}$$

The '*p*' vector features for the '*x*' field cumulative contribution rate are

$$\mathrm{P}_i = \sum_{i=1}^{p} \lambda_i / \sum_{i=1}^{m} \lambda_i, \tag{12}$$

where '*m*' represents the number of sites.

The cumulative variance of contribution rate of the 14 droughts reached 85%. The convergence speed of the load vector was slow due to the extension of the study area, complex topography, differences in the spatial distribution of drought disasters along with significantly larger variability. Additionally, each load vector still retains information about the main characteristics of the study area's drought disasters. North et al. (1982) succeeded in calculating the error range of the features for a significant test. The error range of the characteristic value λ_j was calculated using:

$$e_j = \lambda_j \left(\frac{2}{n}\right)^{\frac{1}{2}} \tag{13}$$

where '*n*' is the sample size. When the adjacent value is λ_{j+1}, then:

$$\lambda_j - \lambda_{j+1} \geq e_j \tag{14}$$

It is considered that these two characteristic values corresponding to the Empirical Orthogonal Function are valuable signals.

2.5. Significance test

The seven IMF components obtained after decomposition can be tested using significance tests to determine whether they belong to pure noise or the physical component in the original sequence (Wu and Huang 2004). By analyzing the distribution of energy spectrum, density, and period of each IMF component, the property of the IMF component is determined, and the required component is determined. The energy spectrum density of the first IMF component is

$$E_k = \frac{1}{N} \sum_{j=1}^{N} |I_k(j)|^2 \tag{15}$$

where N represents the length of the component, and I_k (j) is the K components of the experiment from the Monte Carlo method for the white noise sequence. The approximate relationship between density and the average period can be obtained from the white noise of the K component of the energy spectrum. For an IMF, it is

$$\ln \bar{E}_k + \ln \{\bar{T}_k\}_a = 0 \tag{16}$$

From the X versus Y plot, the relationship between the two will be shown as the slope of the line (the value is -1). In theory, the white noise IMF component should be distributed on the line, but in actual application, there will be some deviation, which gives the white noise energy spectrum distribution of the confidence interval:

$$\ln \bar{E}_k = -\ln \{\bar{T}_k\}_a \pm \alpha \sqrt{2/N} e^{\ln(\{\bar{T}_k\}_a/2)} \tag{17}$$

2.6. Space sensitive areas

Due to the spatiotemporal changes of drought disasters in North China during the Ming and Qing Dynasties, the model composition of the EOF variance contribution rate is low with limited convergence speed as well as complexity or abnormality in sub-regional features. To further discuss regional features, this section was based on the EOF decomposition of the REOF analysis. There are three (3) methods to determine the value 'p' of EOF (Wei 1999). An 85% cumulative variance contribution rate was used in this paper as the standard to determine 'p'. In this paper, the first 14 features of the vector rotation were used. The characteristics of the vector variance distribution after rotation was relatively uniform (Table 2). According to the principle of rotation of factor analysis, the main factor responsible for the geographical distribution of high loads serves as an important basis for the partitioning.

Table 2. Variance contribution rate and cumulative variance contribution rate of EOF and REOF of the first 14 drought disaster models in North China during the Ming and Qing Dynasties.

Model number	EOF		REOF	
	Variance contribution rate /%	Cumulative variance contribution rate /%	Variance contribution rate /%	Cumulative variance contribution rate /%
1	29.37	29.37	9.93	9.93
2	7.91	37.28	4.70	14.63
3	7.57	44.85	7.50	22.13
4	6.14	50.99	5.84	27.97
5	4.75	55.74	10.57	38.54
6	4.26	60.00	6.50	45.04
7	3.99	63.99	4.88	49.92
8	3.59	67.58	5.54	55.46
9	3.46	71.04	5.02	60.48
10	3.41	74.45	5.00	65.48
11	3.05	77.50	4.68	70.16
12	2.97	80.47	5.39	75.55
13	2.74	83.21	4.95	80.50
14	2.69	85.90	5.40	85.90

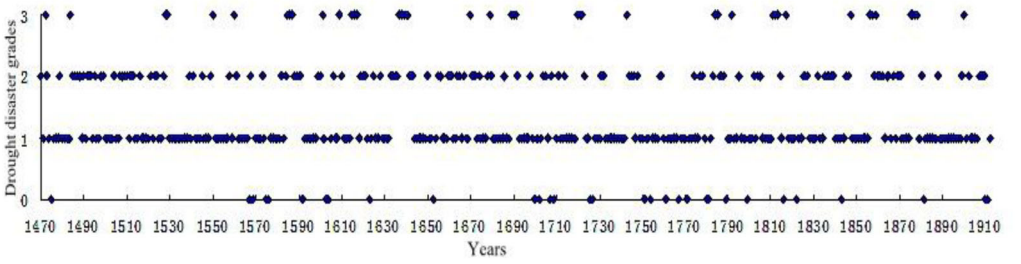

Figure 4. Grade changes of Drought Disasters during Ming and Qing Dynasties (1470-1912) in North China.

3. Results

3.1. Temporal signature analysis: Frequency variation of drought disaster

During the 443 years of the Ming and Qing Dynasties era in North China, 245 general drought disasters, averaging one every 1.8 years were recorded. Among this total, there were 123 severe drought disasters, averaging one every 3.6 years. 44 catastrophic drought disasters, averaging one every 10.0 years (Figure 4) were recorded. Drought disasters with the aforementioned grades, thus, grade 1, 2, and 3 accounted for 59%, 30% and 11% of the total number of drought disasters respectively. The results are in congruence with the study conducted by Cheng and Zhang (1993) entitled: 'Drought and waterlogging classification and its dynamic change in North China'. This study indicated: 'Per statistics over the past 500 years in North China, there is an occurrence of drought every 3 years, highlighting the occurrence of severe drought once in every 10 years'. An index of 0 was assigned to periods, usually years with no drought occurrence. In Figure 4, it can be observed none of the years had a zero index for the period between 1470 AD and 1570 AD. Subsequent era (post-1470 AD and 1570 AD) recorded 0 index between 1750 AD and 1790 AD, indicating the occurrence of fewer drought disasters.

The anomaly value of the drought disaster grade sequence in North China during the Ming and Qing Dynasties was calculated based on the drought disaster grade values data. The five-year, ten-year, and thirty-year moving average of the sequence of drought disaster grade was compiled and plotted, as illustrated in Figure 5. From the thirty-year moving average in Figure 5, it can be observed that drought disasters occurred more frequently in North China from 1499 − 1539 AD, 1606 − 1701 AD, and 1821 − 1912 AD. Contrarily, 1540 − 1605 AD, as well as 1702 − 1820 AD, recorded fewer droughts. According to the thirty-year moving average, the two highest values were obtained in 1644 AD and 1880 AD.

From the five-year moving average, the severity of the drought was high between 1635 AD and 1645 AD. The said era recorded the most serious drought event, with a sliding average of 1.59. However, 1585 − 1592 AD, 1857 − 1871 AD as well as 1876 − 1881 AD experienced low severity of events, with its highest sliding average reaching 1.19. The average value of the moving average reached 1.99 in 1616 − 1622 AD, 1689 − 1695 AD, 1721 − 1725 AD, 1785 − 1789 AD, and 1812 − 1817 AD.

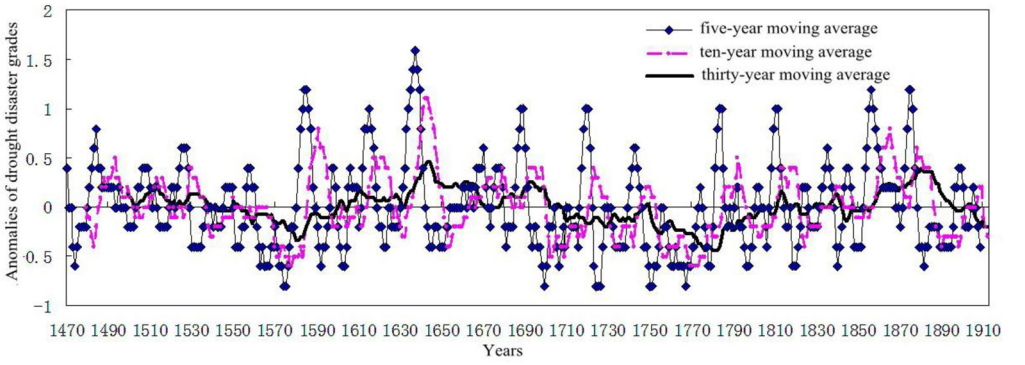

Figure 5. Moving average of grade anomaly value during the Ming and Qing Dynasties (1470-1912) in North China.

From the ten-year moving average, it can be observed that drought event experienced between 1636 AD and 1650 AD was the most serious, with a sliding average of 1.09, which in general aligns with the periods of most serious drought from the five-year moving average. In contrast, periods with low severity were from 1586 to 1596 AD as well as 1858 to 1873 AD. The highest sliding average for the given periods reached 0.79.

Based on the aforementioned study results, it can be concluded from the three curves that periods experiencing or recording high severity levels of drought disasters during the Ming and Qing Dynasties in North China were 1586—1592 AD, 1635—1645 AD, as well as 1858—1871 AD.

3.2. Intensity change in drought disasters

To understand the change in drought disasters in North China during the Ming and Qing Dynasties, the frequency, intensity and anomaly of drought disasters were calculated every 20 years, as shown in Figure 6. Drought disaster frequency level reflects the degree of drought disaster-prone areas, hence, cannot reflect the intensity of droughts. The present study employed the weighted average method to calculate the average intensity level for each 20-year drought value, using the formula (Gao and Zou 2013):

$$I = (a + 2b + 3c)/(a + b + c) \tag{18}$$

The parameter, I, indicates the average grade of drought disaster intensity in North China for the 20 years. a, b, and c, respectively, connotes the frequency of drought disasters pertaining to grade 1, 2, and 3 in North China for every 20 years. The anomaly value of several drought frequencies was positive, indicating a high drought disaster occurrence rate for the given period. Again, a negative anomaly indicates that a drought disaster in that period is less likely. If the intensity of the drought disaster is positive, the intensity of a drought disaster in this period would be higher whilst if negative, the intensity would be lower.

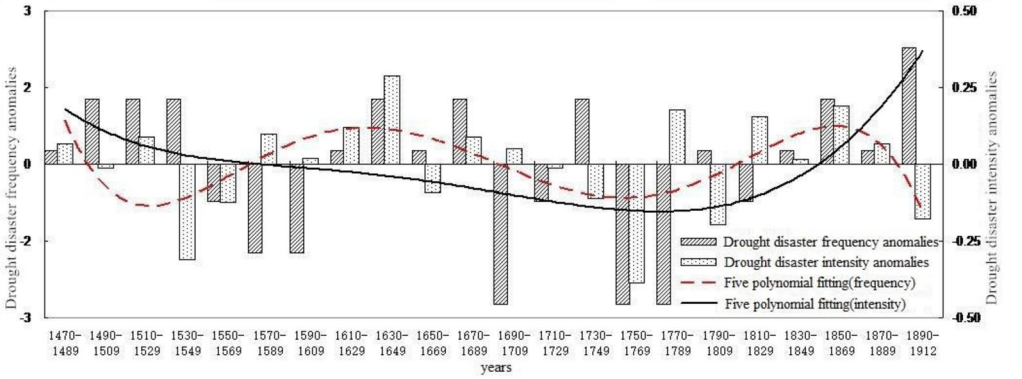

Figure 6. Drought disaster frequency and intensity anomalies in North China in the Ming and Qing Dynasties and their fifth degree polynomial fitting.

Several drought disaster frequencies, anomalies and intensities were positive, which shows that the degree of intensity of drought disaster was greater and more serious in those periods (as shown in Figure 6, the case scenarios for the given periods: 1510－1529 AD, 1610－1629 AD, 1630－1649 AD, 1670－1689 AD, 1470－1489 AD, 1830－1849 AD, 1850－1869 AD, and 1870－1889 AD). The 1630 AD to 1649 AD as well as 1850 AD to 1869 AD periods experienced the most serious drought disaster events, especially the period of 1630 AD to 1649 AD. Despite the existence of relevant literature concerning the scope of this study, history of drought disasters and their durations in the Chongzhen period are rare (Sheng 1990).

According to the principle of the classic least square method (Feng et al. 2001), the trend line is fitted to reflect the change in drought frequency and intensity for North China during the Ming and Qing dynasties for the 20-year scale. As depicted in Figure 6, the drought disaster frequency fitting the fifth-degree polynomial increased after a decline. This reflects the drought disasters in North China during the Ming and Qing Dynasties on a 20 year-scale, experiencing such fluctuations with the mutation time occurring during the Qianlong period (1770－1789 AD). Prior to this period, the degree of drought disaster declined steadily. The trend of the decline was sluggish. After 1789 AD, the degree of drought disaster increased gradually, and the trend of this increase was faster. The intensity curve shows the fluctuation of drought intensity on a 20-year scale. As shown in Figure 6, there were two droughts periods in North China during the Ming and Qing Dynasties, with serious repercussions. One of the said periods occurred in mid-to-late Ming Dynasty (1570 AD), whilst the other event occurred during the mid-to-late Qing Dynasty (1810 AD). Therefore, the variation in the intensity of drought disasters during the Ming and Qing dynasties can be divided into four stages. The first stage was from 1470 AD to 1569 AD, when the drought severity was mild; the second stage was from 1570 AD to 1689 AD, when the drought disaster was very serious; the third stage was from 1690 AD to 1809 AD, when drought severity was mild; and the fourth stage was from 1810 AD to 1912 AD, when drought disaster was very serious. Regardless of results obtained for moving average or polynomial fitting (as depicted in Figure 5 and 6), evidence of the occurrence of the two droughts could be observed during the

Chongzhen as well as from Daoguang to Tongzhi periods. However, the drought that occurred between 1586 AD and 1592 AD in the moving average curve did not reflect in the polynomial fitting curve. In Figure 6, the anomaly values of drought disaster intensity were positive, while the anomaly values for drought disaster frequencies were negative for 1586-1592 period. This shows drought disasters occurred less frequently despite the high severity in the aforementioned period.

3.3. Multiple time scale changes for drought disasters

The noise ratio and the sampled number of perturbed white noise, as well as the original signal used in the ensemble decomposition, are 0.2 and 100. These values were used for resolving boundary problems in the EEMD decomposition process. The mirror extension method was used to arrange the data at both ends of the symmetric extension. This gives a better solution to the boundary (Huang et al. 2003) in the decomposition process of EEMD to address the phenomenon of underestimation.

The EEMD method provides seven cycles with different IMF components (IMF 1−7) and a RES, as shown in Figure 7.

Each IMF component contains a different frequency from high to low, which shows that the drought grade sequence contains multiple time scale characteristics, and each component sequence reflects the localization characteristics of the original sequence. The resulting RES represents the changing trend of the original data sequence over the total time horizon. In Figure 7, the IMF components have a relatively stable period. In the same period, quasi-periodic oscillations with different time scales also showed strong or weak non-uniform changes. The average of each cycle, the variance of the original data for the contribution rate, and the correlation between each IMF component with the original sequence are calculated and presented in Table 3.

Figure 7 shows the amplitude and fluctuation amplitude of IMF1 are the largest among the seven decomposed components. The amplitude of the IMF components decreases steadily whilst the wavelength amplifies accordingly. Over the entire period, the fluctuation of the IMF component tends to be steady with the increase in order. The RES in Figure 7 shows a slightly increased and a decreasing trend over the entire period with no obvious cycle change. It may be part of a longer cycle. In emergence with the polynomial fitting in Figure 6, we can observe the changes in the seventh component (IMF7) as intensity for the drought disaster for the fifth-degree polynomial fitting curve has similar variation trend, showing fluctuations in the time scale over the given period. The peaks and troughs appear more favourable. The changing trend of drought disasters in North China is consistent with the analysis results of the EEMD, which provides credibility and important basis for drought disaster trend analysis in North China during the Ming and Qing Dynasties.

Combining the information in Figure 7 and Table 3, we found out that there are three major time scales for drought disaster in North China during the Ming and Qing dynasties:

(1) On the inter-annual scale, there are periodic fluctuations with an average period of 3 years (IMF1) and 6.1 years (IMF2). The variance contribution of IMF1 (3-

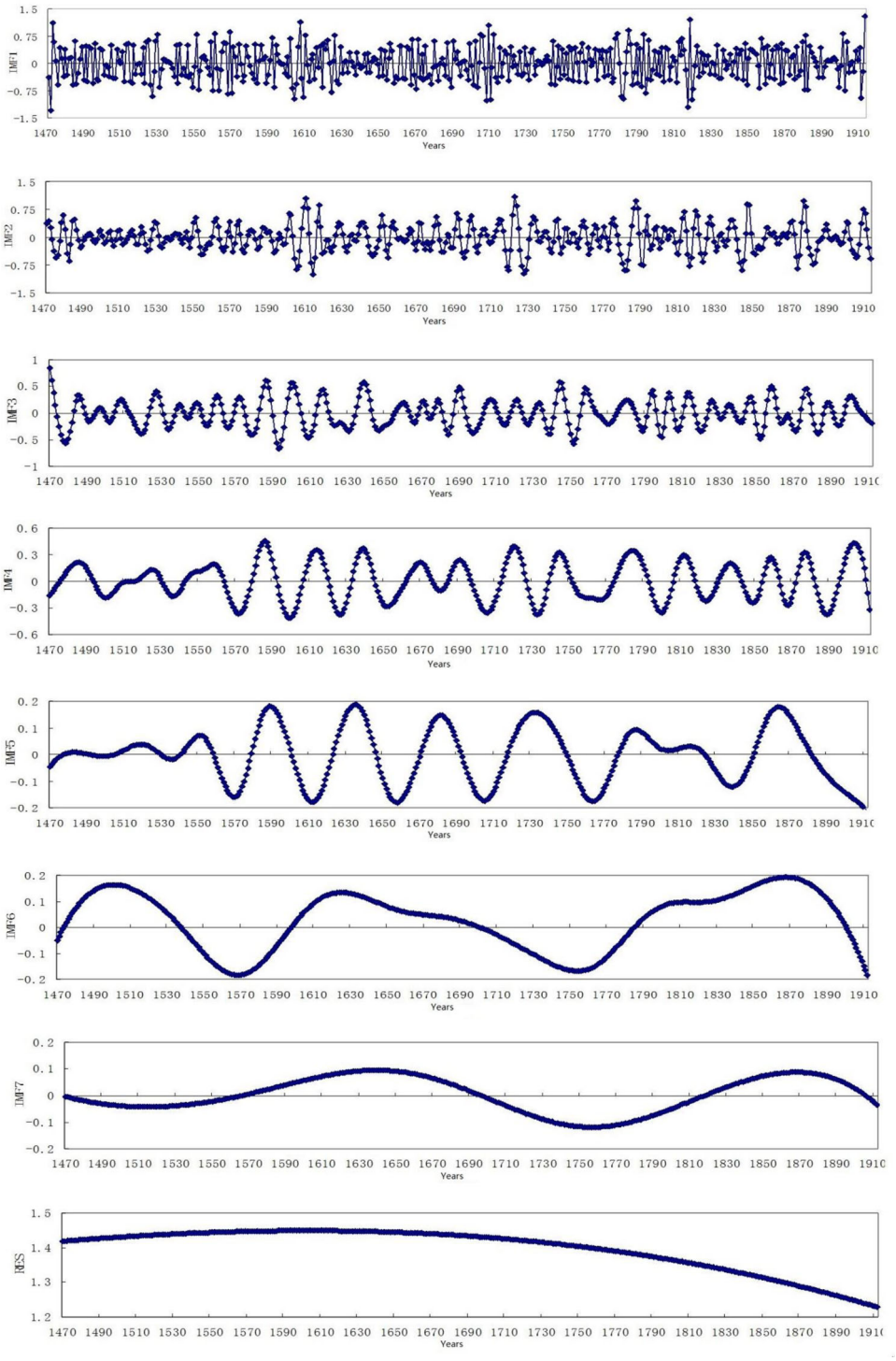

Figure 7. EEMD decomposition results of drought disaster grade sequence in North China in the Ming and Qing Dynasties.

Table 3. Cycle, correlation coefficient, and variance contribution rate of each component in the drought disaster grade sequence in North China in the Ming and Qing Dynasties.

IMF component	IMF1	IMF2	IMF3	IMF4	IMF5	IMF6	IMF7	RES
Cycle / year	3.0	6.1	12.7	27.4	48.4	151.1	214.5	
correlation coefficient	0.61**	0.60**	0.49**	0.37**	0.21**	0.18**	0.15**	0.013
The contribution rate /%	21.4	16.9	14.6	12.7	12.3	9.4	8.0	4.7

Note: ** Significance level of 1%.

year cycle) reached 21.4%. The obvious oscillation signal of IMF1, except for a few years, had large-amplitude, with the amplitudes of the remaining periods relatively stable. The periods with greater amplitude were 1470－1475 AD, 1605－1610 AD, 1708－1712 AD, 1810－1815 AD, and 1910－1912 AD. IMF2 had a variance contribution for the 6.1-year cycle at 16.9%, as the amplitude was greater in some periods. The larger amplitude periods were 1608－1613 AD, 1710－1720 AD, 1780－1790 AD, 1840－1845 AD, and 1870－1880 AD. Between 1490 AD and 1600 AD, the amplitudes were small. Referring to relevant data, it was revealed that during periods of small amplitude in IMF1 and IMF2, the occurrence of drought disasters was less; thus, IMF1 and IMF2 reflect the original sequence more realistically. The distribution (Table 3) shows the correlation coefficients between the two components of IMF1 and IMF2. The original sequence for both components were 0.61 and 0.60, respectively, passing the significance level test of 0.01. This indicates their change characteristics have a high similarity with the drought disaster's original rank data sequence.

(2) On the inter-decadal scale, there are periodic fluctuations in the mean period of 12.7 years (IMF3), 27.4 years (IMF4), and 48.4 years (IMF5). The contribution rate of variance of the IMF3 component was 14. 6% with a larger amplitude between 1580 AD and 1650 AD. The amplitude for the entire period differed a bit against a relatively mild fluctuation in time-scale. The variance contribution rate of the 27.4-year cycle, represented by IMF4 was 12.7%. This revealed between 1470 AD and 1550 AD, the amplitudes were smaller than those recorded for other periods. This shows drought disasters occurred less frequently during the 27.4-year cycle between 1470 AD and 1550 AD. IMF5 had a variance contribution rate of 12.3% for a 48.4-year cycle; except for the period1470 AD- 1550 AD. In addition, the 1780 AD to 1830 AD era had some level of consistency in the fluctuations. From 1470 AD to 1550 AD, the IMF5 component fluctuated around zero, indicating a less severe period of drought disasters. From 1780 AD to 1830 AD, volatility relative to the entire period was minimal, indicating a period of drought disaster with low magnitude.

(3) On a century-scale, there was the existence of fluctuations for 151.1 years (IMF6) as well as 214.5 years (IMF7). Their variance contribution rates were 9.4% and 8%, respectively. The IMF6 and IMF7 gradually approached the trend of RES, adhering to a residual trend for the two components. The decomposition of EEMD (the residuals and the average value of the difference in the trend of integration) reflects the drought disaster grade sequence over the entire time-scale (Wang and Li 2011). At the same time, looking at the correlation coefficients in Table 3, it was found that the correlation coefficients between each IMF component in the low-frequency class and the original rank data sequence were smaller. This may be partly down to the period of low-frequency component being relatively long as the trend direction changes slowly. When the original data sequence has an upward trend (or

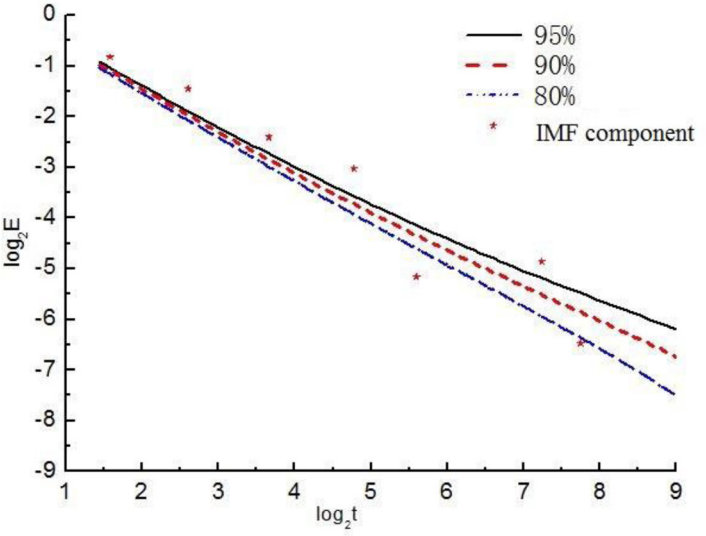

Figure 8. Significance test of each IMF component signal of drought disaster grade sequence in North China during the Ming and Qing Dynasties.

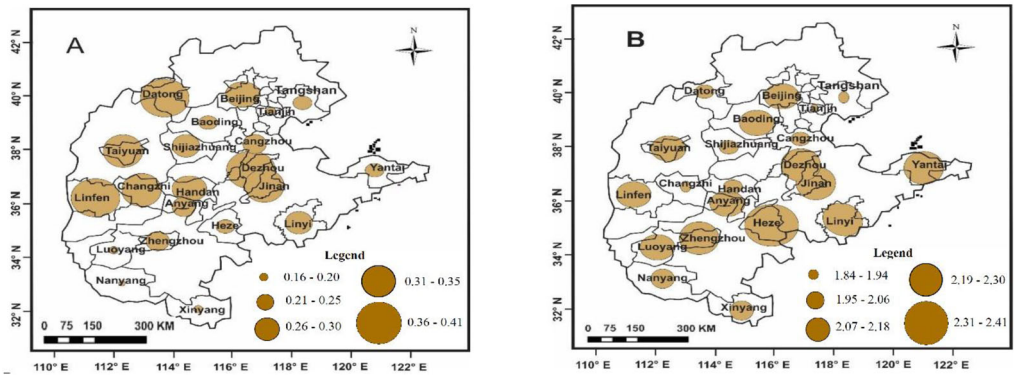

Figure 9. Frequency of drought disasters in North China during the Ming and Qing Dynasties (1470–1912). (A) Frequency distribution map, (B) Intensity distribution map.

downward), the low-frequency component type according to the direction of the original operation will continue over a given period before a change in direction. This eventually results in variations in volatility that is often contrary to that of the original time series.

4. Discussion

4.1. Spatial distribution analysis: Spatial distribution of frequency and intensity of drought disaster

Statistics on drought disasters were obtained for 21 sites during the Ming and Qing Dynasties in North China for the given period (443 years). A map showing the drought disaster frequency distribution was created (Figure 9A). The circles represent

the frequency and occurrence of drought disasters. The greater the radius, the higher the frequency of the drought. Linfen recorded the highest drought frequency among the 21 study sites (up to 181). This means 181 drought disasters occurred over the study period (443 years). The occurrence rate was 40.9%, on average, there was drought every 2.4 years. Nanyang recorded the smallest drought frequency, where 69 droughts were recorded, accounting for 15.6%; showing a drought disaster occurred every 6.4 years. Therefore, drought disasters were more frequent with high level of severity in North China.

The present study adopted the weighted average method to calculate drought intensity and the average grade for each site based on the expression used in a similar scenario by Gao and Zou (2013). The expression below was employed mainly due to frequency of drought disasters solely reflecting regional data and not size and density. Hence, adopted to capture such details as stipulated by Gao and Zou (2013):

$$I = (a + 2b + 3c)/(a + b + c) \tag{19}$$

where I represent the drought intensity and average grade for each county and a, b, and c are 1, 2, and 3 occurrences of drought, respectively.

Figure 9B shows the distribution of drought intensity at 21 sites in North China during the Ming and Qing Dynasties. The circles represent the intensity of drought disasters. The greater the radius of the circle, the greater the drought intensity. The figure shows the highest drought disaster intensities in Eastern North China in the Shandong Dezhou, Jinan, Heze, Linyi, and Yantai districts. Besides, the drought intensity in North China was the lowest in the northeastern part of Tianjin and Tangshan and Hebei, Handan, Cangzhou, and Shijiazhuang. There was no correlation between drought disaster frequency and intensity. The frequency of drought disasters was higher in the Shanxi District; however, the intensity was relatively low, which meant drought was not serious, although drought occurrence frequency was high in the area. The frequency of drought disasters was smaller in Shandong Province (Heze, Yantai, and Linyi), but the intensity of the drought disasters was huge. This means rate of drought occurrence was low but the few that occurred had severe consequences in these areas. Contrary to the aforementioned areas in Shandong province, Dezhou and Jinan areas, unlike the others, experienced high frequency and intensity in drought disasters. This indicates these two areas are susceptible to droughts.

According to An et al. (2014), the past 50 years of drought disasters in North China has revealed the zone with high frequency was mainly located in middle to the southern zone of North China considering the spot location identified in Hebei. A large value of cumulative intensity value was observed in middle to the southern zone of North China, including Hebei, Henan and Shandong. The results of this paper indicate the different frequency and intensity distributions for the droughts in North China during the historical periods. Figure 9 shows the drought intensity was relatively high in Hebei, Henan, and Shandong, the three provinces of the border area near Heze, Jinan, and other regions. The current study is in congruence to the study conducted by An et al. (2014) bearing certain similarities, hence, indicating that

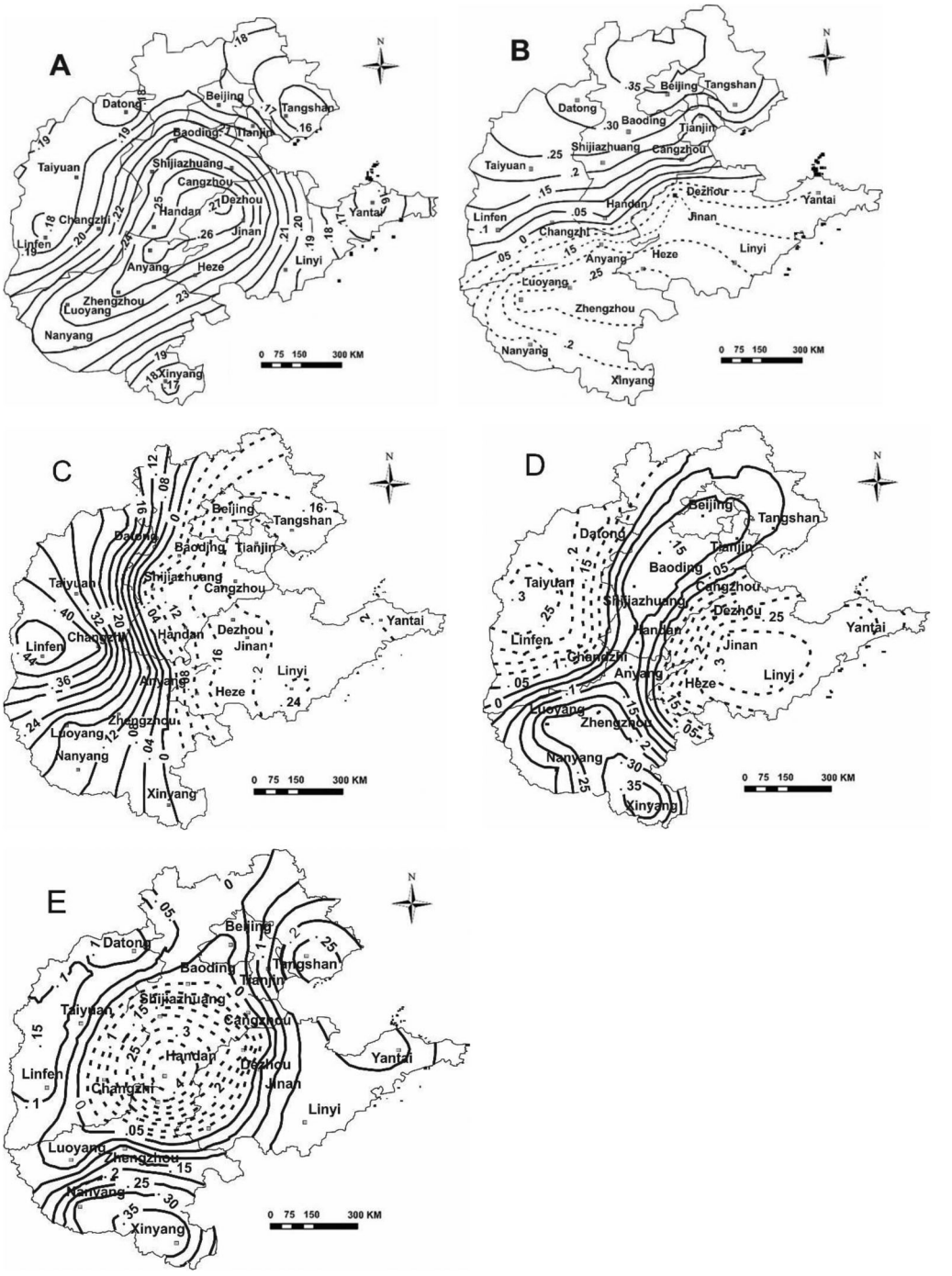

Figure 10. The EOF decomposition of the drought grade sequence in North China during the Ming and Qing Dynasties (A. first model; B. second model; C. third model; D. fourth model; and E. fifth model).

droughts recorded in recent years differ from other drought disasters, that were recorded centuries ago. However, there was general consistency in variation. The study of drought disasters during the historic period is still of great significance to current and future drought researches.

4.2. Spatial modal distribution of drought disaster

In the first five modes through the significance test model, the cumulative variance contribution rate was 55.74% (Table 2). Hence this article analyzed the given five modes of spatial distribution. The first model of the maximum contribution rate of the variance is the highest and reflects the spatial distribution of the droughts best. The spatial distribution of the first model shows that the drought disasters in North China during the Ming and Qing Dynasties were consistent across the whole region (Figure 10A). This shows changes in the droughts for the region are identical (uniform), showing more or less slight characteristics. The large load value area was located in Dezhou in the Shandong Province, which means the region has the most variable drought disaster rate. The variance contribution of the first model was 29.37%, reflecting a more important contribution rate of drought disasters in North China. The changes in the time series and grade sequence are almost identical in North China. The correlation coefficient was 0.904 and the significance test value was 0.01. This shows the first model appropriately reflects the distribution of drought disasters in North China. The second model entailed a spatial distribution field model (Figure 10B). The first and second feature fields differed significantly. The N–S spatial structural features were the opposite. For instance: results revealed opposite ends, thus, when severity level is high in the south, it turns out to be low in the north and vice versa. The zero line was located between 36°N–38°N crosses the Changzhi, Handan, and Dezhou districts. The centre of the maximum value was located at the centre in the northern part of Beijing District in North China. The centre of the maximum negative value was located in the south of Henan Province in Zhengzhou and Luoyang districts. The third spatial distribution field model (Figure 10c) shows the drought's spatial structure features of North China were reversed during the Ming and Qing Dynasties. The zero line was located between 114°E–115°E, connecting Xinyang and Handan districts. Its maximum centre value was located in Shanxi and Linfen districts in the western region of North China; the maximum negative centre was located in the eastern Shandong Linyi districts in the northeastern part of North China. The fourth spatial distribution field model (Figure 10d) indicates that the spatial structure drought features are reversed in northern/south–southeastern part of North China during the Ming and Qing Dynasties. There are two positive and negative centres. The centre of the maximum of the two positives values in the northern part of North China was in Hebei and Shijiazhuang, Baoding, and the southern part of Henan and Xinyang districts. The two-maximum negative centres are in the Shanxi and Taiyuan districts in the western part of North China as well as in Shandong, Jinan, and Linfen in the eastern part. The fifth model spatial distribution field (Figure 10e) implies opposite characteristics for the drought in the north-central region compared to the surrounding area (the middle – around reverse type). The

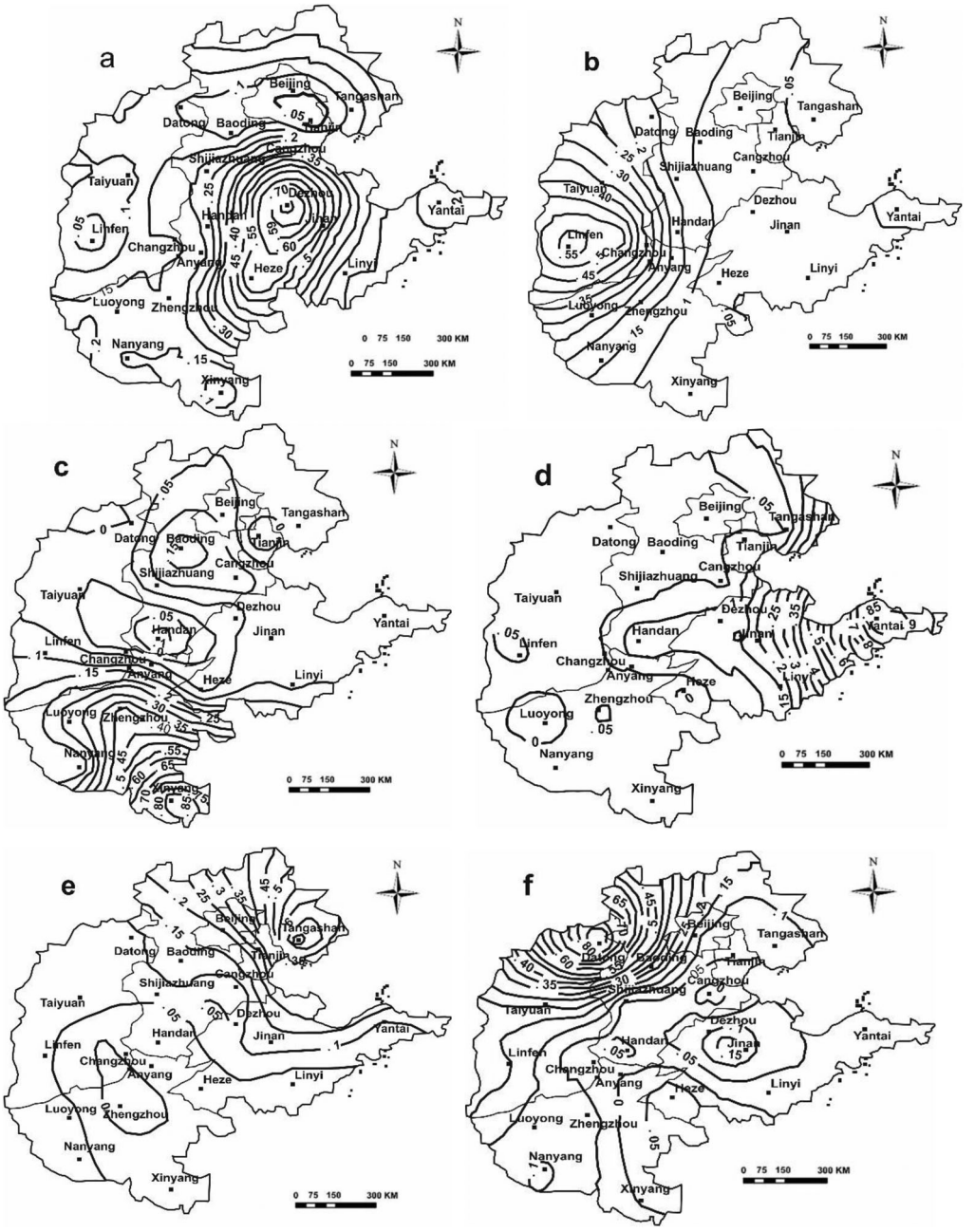

Figure 11. REOF drought rank sequence decomposition of North China during the Ming and Qing Dynasties (a. The 1st rotation vector; b. the 2nd rotation vector; c. the 3rd rotation vector; d. the 4th rotation vector; e. the 5th rotation vector; and f. the 6th rotation vector).

centre of the maximum negative value was located in Hebei and Handan in the northcentral region. The centre of the maximum value was located in the Tangshan, Hebei, Shandong Laiyang, Shanxi Linfen, Xinyang, and Henan districts.

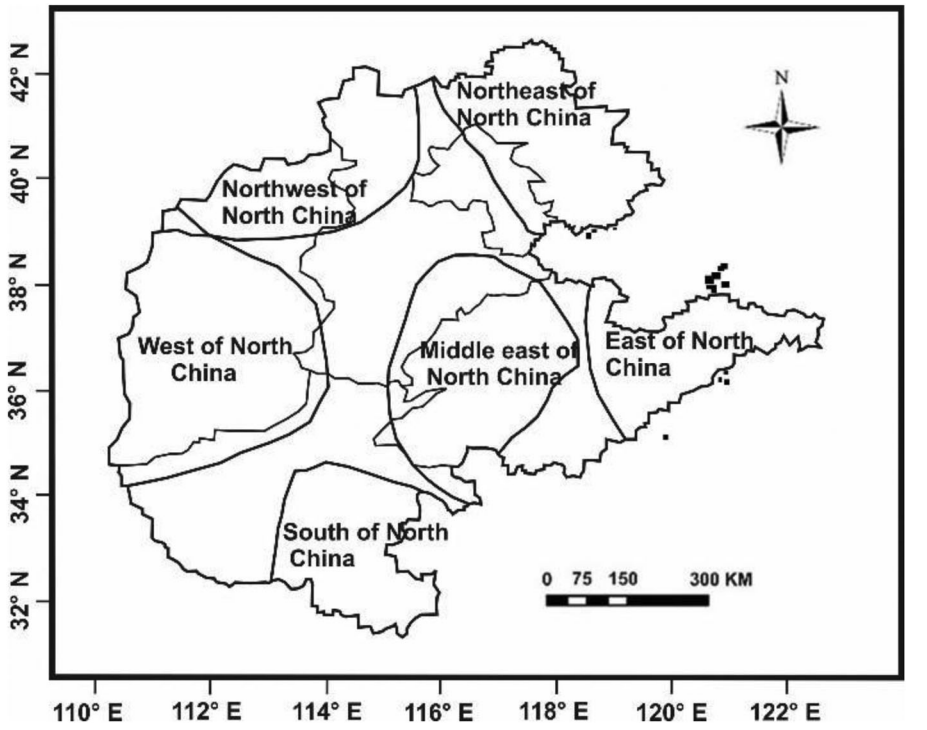

Figure 12. Schematic partition of the REOF analysis of droughts in the Ming and Qing Dynasties in North China.

4.3. Space sensitive areas

Using the significance test, the results show that the first six modes passed the significant test. The distribution of the first six (6) main factors was presented in Figure 11. The variance contribution rate of the 1st rotation vector (RLV1) was 9.93%. Large values were mainly observed in the eastern part of North China; the maximum value of the rotational load vector was observed in Shandong and Dezhou in the eastern part of North China. This model was captioned as the 'Eastern North China model' as illustrated in Figure 11a. The variance contribution rate of the 2nd rotation vector (RLV2) was 4.70%. Large values were mainly observed in the western part of North China; the maximum rotational load vector was located in Shanxi and Linfen in the western part of North China. This model was captioned as 'Western North China model' as illustrated in Figure 11b. The variance contribution rate of the 3rd rotation vector (RLV3) is 7.50%. Large values were mainly observed in the southern part of North China; the centre of the maximum rotational load vector was located in Henan and Xinyang areas in the southern part of North China. This model was captioned as 'Southern North China model' as depicted in Figure 11c. The variance contribution rate of the 4th rotation vector (RLV4) was 5.84%, with large values in the eastern part of North China and the centre of the maximum rotational load vector in Shandong and Laiyang in the eastern part of North China. This model was referred to as

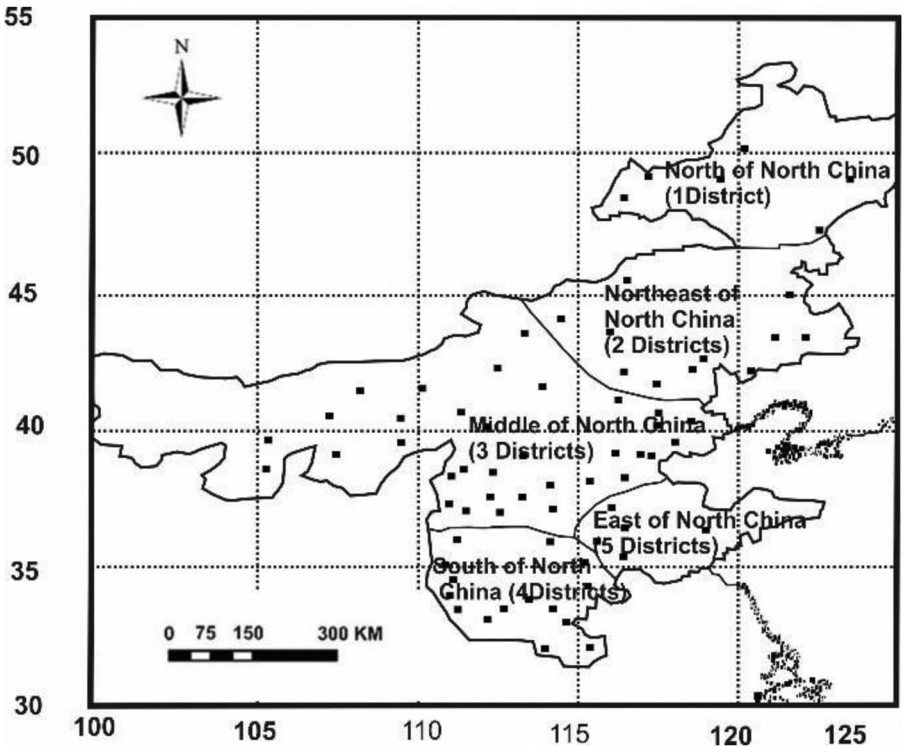

Figure 13. Partitions of five regions of rainfall in North China according to Rong Y. (2004).

'Eastern North China model' as presented in Figure 11d. Shandong is located close to the Bohai and Yellow seas in the Yellow River Delta. It is characterized by abundant rainfall and fewer drought areas. The variance contribution rate of the 5th rotation vector (RLV5) was 10.57%, with large values in the northeastern part of North China and the centre of the maximum rotational load vector in Tangshan of the northeastern part of North China. This model was referred to as the 'Northeastern North China model' as presented in Figure 11e. The variance contribution rate of the 6th rotation vector (RLV6) was 6.50%, with large values in the northern part of North China and the centre of the maximum rotational load vector in Shanxi and Datong in the northwestern part of North China. This was captioned as the 'Northwestern North China model' as illustrated in Figure 11f. This area hosts more relief (mountains, hills and so on) features. The Great Wall is located in the north, characterized as a dry area with high level of drought severity. The drought in North China can, therefore, be divided into six regions: middle–east of North China, the western part of North China, the southern part of North China, the eastern part of North China, the northeastern part of North China, as well as northwestern part of North China. Since the REOF method can appropriately reflect the local characteristics of droughts in North China, the absolute value of the high load area in the space of each model was higher. The regional characteristics of North China are intuitively reflected. Figure 12 is a schematic diagram of the six modes of REOF decomposition of the drought in North China. The northeastern part of North China was identified as the most sensitive region, followed by middle–east of North China.

Rong (2004) considered the climate of North China based on different angular divisions and studied the precipitation of the region from 1957 AD to 2002 AD. He used a similar method to determine the rainfall in North China, further categorizing it into five (5) regions constituting the northern part of North China, the northeastern part of North China, the middle part of North China, the southern part of North China, and eastern part of North China (Figure 13). Rong (2004) removed the northern part of the North China region and discussed the remaining four (4) mainly due to the differences that existed within the study area. In our article, middle North China was divided into middle–east of North China, the western part of North China as well as the northwestern part of North China.

4.4. Significance test

Per the expression given in Equation (17), the term a, was the significance level. As shown in Figure 8, the curves with significance levels of $a = 0.05$, 0.10, and 0.20 are given. If the IMF component is above the confidence curve, the component has passed the significance test, and it is considered that the component contains information with actual physical meaning in the selected confidence level range. If the decomposed IMF component is below the confidence curve, the component has not passed the significance test. The physical meaning of the component is relatively small, and the information is mostly white noise.

Values closer to the left indicate the higher frequency and a smaller cycle. The vertical axis represents the energy spectral density of the decomposed IMF component. The closer the upper component is, the higher the energy it has, along with greater amplitude. From the chart, we can see that IMF1, IMF2, IMF3, IMF4, and IMF6 fell in the 95% confidence interval, indicating that these components were significant. The physical meaning of these components includes the information for the main period of the oscillation cycle corresponding to the drought disaster grade sequence dry area in North China during the Ming and Qing Dynasties. This is in agreement with the study findings of Wu and Huang (2004). IMF5 and IMF7 fell on the 80% confidence interval, indicating less physical meaning for the two components. The cycle related to these two scales show relatively weak energy in the process of drought disaster change in North China during the Ming and Qing Dynasties.

Moreover, it could be noticed from the various year cycles, thus, a 48.4-year cycle of IMF5,151.1-year cycle of IMF6, and a 214.5-year cycle of IMF7 that 1630－1649 AD, as well as 1850－1869 AD, are in a positive phase. These two periods of drought disaster were relatively heavy and consistent with the results of the analysis above. It shows that for the two most serious drought disasters during the Ming and Qing Dynasties, the response of North China was obvious in the 48.4-, 151.1-, and 214.5-year cycles. The Beijing meteorological station has analyzed the changes and trend of drought and waterlogging in Beijing over the past 500 years. The results showed that during the Ming Dynasty from 1484 AD to 1643 AD (160 years) as well as the 45 years (from 1536 AD to 1580 AD) received average rain, whereas the remaining 115 years received less rain (Beijing Observatory 1977). However, this analysis was based on the annual rainfall situation, recorded for the given period. If precipitation

in winter and spring was solely considered, drought occurred between 1536 AD and 1580 AD (Gao 2003). From each component of the EEMD decomposition, it can be seen that the period of 151.1 years was the most significant. IMF7 between 1536 AD and 1580 AD (in the negative phase of the period of 214.5 years) was also significant. Based on the previous analysis of meteorological data from the Ming Dynasty, China's climate began to turn cold from the fourteenth century. After the fifteenth century, the climate became colder (Zou 1995). Along with the constant cold climate, North China entered a relatively dry stage, known as the 'small ice age of the Ming and Qing dynasties'. The Ming Dynasty encountered a 'Little Ice Age' with very cold winters, especially at the latter part during the Ming Dynasty era from 1580 AD to 1644 AD. Studies have shown that this period of cold was the coldest in one thousand years, in ten thousand years, and one million years. In other words, since the beginning of human civilization, the end of the Ming Dynasty was the coldest period (Cai and Yin 2009). A study on disasters in Guanzhong area during the Ming and Qing Dynasties, revealed during the little ice age, the frequency of the occurrence of drought and frost was synchronous. The disasters that occurred most frequently within this period were drought disasters (Cai and Yin 2009). Since the beginning of 1580 AD, the components of IMF6 were in the negative phase with a positive phase transition. IMF4 and IMF5 were in the negative phase transcending to a transitional stage whilst IMF7 were in a positive phase, indicating the period of drought disaster was more serious associating this process to the 'Little Ice Age'. For the small ice age during the Ming and Qing Dynasties, the response in North China was obvious in the 27.4-, 48.4-, 151.1-, and 214.5-year cycles.

5. Conclusions

The present study provides detailed information about the spatiotemporal characteristics of drought disaster in North China during the Ming and Qing dynasties. The results or main findings show that:

i. The occurrence of drought disasters are recurrent and more severe in northern and low in the southern part of North China. Reasons were mainly attributed to the degree of evaporation, limited transportation of water vapour from the East Monsoon of the Pacific Ocean and abnormal atmospheric circulation causing variations in temperature and precipitation.
ii. In general, drought intensity distribution was high in the southeastern part of North China and low in the northwestern part. Changes in drought disaster were uniform across the selected areas used for this study.
iii. Using EOF and REOF methods, the drought disaster in the study area during the Ming and Qing Dynasties, the overall results of the study revealed drought disasters were classified into four (4) stages based on the two catastrophic events that occurred during the mid-to-late periods of both reigns. Formation and occurrence of drought disasters often take time with varying degree of impacts as well as composition (light to heavy).

Considering the increasing concerns of food security, growing population and deterioration of forest cover/vegetation, lack of detailed information on historical population and socio-economic factors that the present study does not capture, further studies could be conducted on historical impacts of socio-economic activities and how they have somewhat influenced the spatial distribution of drought disasters in the study area. Again, subsequent studies could delve into sunspot activity and ENSO from the Pacific Ocean, which are key climatic factors that adversely influence the occurrence of droughts in different areas.

Acknowledgements

This work was supported by the National Natural Science Foundation of China (Grants -41971340 and 41271410). The authors would like to thank the handling editor and anonymous reviewers for careful reviews and helpful remarks.

Author contributions

Shuoben Bi, Changchun Chen, and Yanping Li conceived and designed the experiments; Yanping Li and Ying Lu performed the experiments; Shuoben Bi, Yanping Li, and Ying Lu wrote the Chinese paper; Shengjie Bi, Ying Lu and Athanase Nkunzimana translated the paper.

Conflicts of interest

The authors declare that they do not have any commercial or associative interest that represents a conflict of interest in connection with the paper they submitted.

ORCID

Shuoben Bi http://orcid.org/0000-0002-7295-1716

References

An LJ, Ren FM, Li YJ, Li YP. 2014. Analysis of the characteristics of meteorological drought events in North China in past 50 years. Meteor. 40 (9):1097–1105.

Beijing Observatory. 1977. Journal of climate change and extreme weather prediction. Beijing: Science Press.

Cai WJ, Yin SY. 2009. The freeze disasters in the little Ice Age of Ming and Qing dynasties in the Guanzhong region. J Arid Land Resource Environ. 23(3):118–121.

Central Weather Bureau in North China. 1975. The historic of nearly five hundred years of drought and flood in North and Northeast of China. Peking University.

Chen YY, Chen N, Wang SG, Qian ZA, Mu JH. 2010. The characteristics of spatiotemporal variation of precipitation in arid and semi-arid area of Mongolia [I]: Annual precipitation characteristics from May to September precipitation with REOF analysis. Plateau Meteor. 29 (1):33–43.

Chen Y, Ying YX, Chen XW. 2011. Change of flood disasters in China since the 1880s and some possible causes. J Nat Resource. 26(12):2110–2120.

Chen ZK, Zhang SY, Luo JL, Li ZR. 2013. A climatic analysis on the precipitation features and anomaly in Northwest China. J Desert Res. 33(6):1874–1883.

Chen XC, Zhang LP, Zou L, Shan LJ, She DX. 2019. Spatiotemporal variability of dryness/wetness in the middle and lower reaches of the Yangtze River Basin and correlation with large-scale climatic factors. Meteorol Atmos Phys. 131(3):487–503.
Cheng H, Zhang RY. 1993. Drought-flood types and their dynamic variation in North China. Scientia Geogr Sinica. 13(2):129–137.
Devkota RP, Pandey VP, Bhattarai U, Shrestha H, Adhikari S, Dulal KN. 2017. Climate change and adaptation strategies in Budhi Gandaki River Basin, Nepal: a perception-based analysis. Clim. Change. 140(2):195–208.
Ding YG, Zhang YC, Liu JF. 2007. A new cluster method for climatic classification and compartment using the conjunction between CAST and REOF. Chin J Atmos Sci. 31(1): 129–136.
Dracup JA, Lee KS, Paulson EG. 1980. On the definition of droughts. Water Resour. Res. 16(2):297–302.
Feng JH, Che GM, Nie YF. 2001. Numerical analysis principle. Beijing: Science Press.
Gaire NP, Dhakal YR, Shah SK, Fan ZX, Bräuning A, Thapa UK, Bhandari S, Aryal S, Bhuju DR. 2019. Drought (scPDSI) reconstruction of trans-Himalayan region of central Himalaya using Pinus wallichiana tree-rings. Palaeogeogr. Palaeoclimatol. Palaeoecol. 514:251–264.
Gao SX. 2003. Dust weather and its contributing factors in Beijing of Ming dynasty. J Beijing Inst Edu. 17(3):33–37.
Gao C, Zou WQ. 2013. Analysis of spatial and temporal characteristics of drought in Fenhe river basin. J Shanxi Univ. 36 (1):21–26.
Han RQ, Gao H, Li WJ. 2014. Application of Rotational Empirical Orthogonal Function method in the prediction and genetic diagnosis of summer temperature in Northeast of China. J Meteor. 72 (2):291–305.
Hao ZX, Wu MW, Liu Y, Zhang XZ, Zheng JY. 2020. Multi-scale temperature variations and their regional differences in China during the Medieval Climate Anomaly. J Geogr Sci. 30(1):119–130.
He B, Lu AF, Wu JJ, Zhao L, Liu M. 2011. Drought hazard assessment and spatial characteristics analysis in China. J Geogr Sci. 21(2):235–249.
Huang NE, Wu ZH. 2008. A review on Hilbert-Huang Transform: the method and its applications on geophysical studies. Rev Geophys. 46(2):1–23.
Huang DJ, Zhao JP, Su JL. 2003. Practical implementation of the Hilbert-Huang Transform algorithm. Acta Ocean Sin. 25(1):1–11.
Katsanos D, Retalis A, Tymvios F, Michaelides S. 2018. Study of extreme wet and dry periods in Cyprus using climatic indices. Atmos. Res. 208:88–93.
Li YH, Li T, Zhao QY. 2000. Spring precipitation in Northwest China and Pacific SSTA autumn characteristics and correlation analysis. Plateau Meteor. 19 (1):100–110.
Li K, Lin X. 1993. Drought in China: Present Impacts and Future Needs. In: Wilhite D.A. (eds) Drought assessment, management, and planning: theory and case studies. natural resource management and policy, vol 2. Boston, MA: Springer.
Li QX, Liu XN, Li XQ. 2002. Study of drought tendency in North China nearly a half century. J Nat Disaster. 11 (3):50–56.
Li J, Qin J. 2013. Analysis of winter drought and atmospheric circulation anomalies in North China. Anhui Agri Sci. 41 (8):3524–3529.
Lin Y, Deng X, Jin Q. 2013. Economic effects of drought on agriculture in North China. Int J Disaster Risk Sci. 4(2):59–67.
Liu L, Xu ZX. 2014. The characteristics and trend of drought and flood forecasting in Southwest China. J Nat Resource. 29 (10):1792–1801.
Liu Y, Ye M. 2007. Regional characteristics of precipitation trend in pre-flood season based on REOF analysis in Guangdong. Guangdong Meteor. 29(4):11–14.
Liu HL, Zhang Q, Wang S, Guo JQ, Yang H. 2014. Spatial distribution and decadal variation of spring season in Hexi corridor. Chin Desert. 34 (5):1386–1392.

Liu WL, Zhang MJ, Wang SJ, Wang BL, Ma XN, Che YJ. 2013. Temporal-spatial variation characteristics of extreme drought events in North China Plain during recent 50 years. Bull Soil Water Conser. 33(4):90–95.
Liu XF, Zhu XF, Pan YZ, Li TQ. 2015. Spatiotemporal changes of drought and their driving forces in North China Plain in the last 54 years. J Beijing Norm Univ. 51(S1):1–7.
Lu P, Dong J, Gao XT. 2016. Temporal and spatial characteristics of drought in North China Plain over the past 55 years based on SPEI. Henan Sci. 34(9):1551–1556.
Ma ZG, Hua LJ, Ren XB. 2007. The North China drought change tendency and the relationship between turning point change and Pacific Ocean decadal oscillation. Chin Sci Bull. 52 (10):1199–1206.
North GR, Bell TL, Cahalan RF, Moeng FJ. 1982. Sampling errors in the estimation of Empirical Orthogonal Function. Mon. Wea. Rev. 110 (7):699–706.
Peel MC, Srikanthan R, McMahon TA, Karoly D. 2011. Ensemble Empirical Mode Decomposition of monthly climatic indices relevant to Australian hydro climatology. Perth, Australia: 19th International Conference on Modelling Simulation.
Piao J, Chen W, Wei K, Liu Y, Graf HF, Ahn JB, Pogoreltsev A. 2017. An abrupt rainfall decrease over the Asian inland plateau region around 1999 and the possible underlying mechanism. Adv. Atmos. Sci. 34(4):456–468.
Rong YS. 2004. Research on explanative wide range of climate change and the drought in North China. Nanjing: Nanjing Institute of Meteorology.
Rong YS, Duan LY, Xu M. 2008. Diagnostic and analysis of persistent drought in North China 1997－2002. Arid Zone Res. 25 (6):842–850.
Shen BZ, Lian Y, Yang HW, Zhang SX. 2012. Inter-decadal change characteristics of summer temperature in Northeast China. Sci Geogr Sinica. 32(6):739–745.
Sheng FY. 1990. Henan historical climate research. Beijing: Chin Meteor Press.
Sun Y, Chen YF, Cheng L, Liu Y, Wei LL, Wang HY. 2012. An analysis and prediction of dry season reservoir in flow based on EEMD. Chin Rural Water Hydropower. (2):34–37.
Sun YF, Lu BH. 2013. The characteristic analysis of precipitation in Nanjing based on EEMD method. Chi Rural Water Hydropower. (3):5–9.
Tang YP, Zhang K, Li ZX, Li L, Sun L, Sun J. 2011. Analysis of climate comfort regional characteristics in Liaoning based on REOF. Environ Sci Technol. 34(2):120–124.
Wang B, Li XD. 2011. Multi-scale fluctuation of European temperature revealed by EEMD analysis. Acta Sci Nat Univ. 47(4):627–635.
Wang P, Wu XQ, Hao YR, Wu CH, Zhang J. 2020. Is Southwest China drying or wetting? Spatiotemporal patterns and potential causes. Theor Appl Climatol. 139(1-2):1–15.
Wang YJ, Yan F. 2014. China regional variation of precipitation and decadal variation from 1960 to 2010. Adv Geog. 33 (10):1354–1363.
Wang XY, Zhuo L, Li C, Engel BA, Sun SK, Wang YB. 2020. Temporal and spatial evolution trends of drought in northern Shaanxi of China: 1960–2100. Theor Appl Climatol. 139(3-4): 965–979.
Wei FY. 1999. Modern climate statistics diagnosis and prediction technology. Beijing: Chin Meteor Press.
Wilhite DA, Glantz MH. 1985. Understanding: The drought phenomenon: The role of definitions. Water Int. 10(3):111–120.
Wu HB. 2005. Diagnosis and prediction of climate variability. Beijing: Chin Meteor Press.
Wu SS, Huang CT. 2015. Prediction of partition precipitation trends of Jiangxi in June based on REOF. Meteor Disaster Reduction Res. 38(1):8–15.
Wu Z, Huang NE. 2004. A study of the characteristics of white noise using the empirical mode decomposition method. Proc. R. Soc. Lond. A. 460(2046):1597–1611.
Xue M. 2007. Theoretical study of population mean empirical mode decomposition method. Harbin: Harbin Engineering University.
Xue CF, Hou W, Zhao JH, Wang SG. 2013. The application of ensemble empirical mode decomposition method in multiscale analysis of region precipitation and its response to the climate change. Acta Phys. 62(10):504–511.

Yang Q, Yao JQ, Zhao Y, Zhao L, Han XY, Zhao L, Huang YZ. 2013. Spatial-temporal variation of water vapor and its relationship with the precipitation in the Ili River basin. J Desert Res. 33(4):1174–1183.

Yi L, Yu HJ, Ge JY, Lai ZP, Xu XY, Qin L, Peng SZ. 2012. Reconstructions of annual summer precipitation and temperature in north-central China since 1470 AD based on drought/flood index and tree-ring records. Clim Change. 110(1/2):469–498.

Zhang DE. 2004. China three thousand years of meteorological record collection. Nanjing: Phoenix Publishing/Jiangsu Edu Press.

Zhang WB. 2009. Floods and drought network database. Chin Water Conser. 5:66.

Zhang DW, Cong ZT, Ni GH. 2013. Comparison of three Mann-Kendall methods based on the China's meteorological data. Adv Water Sci. 24(4):490–496.

Zhang J, Sun FB, Liu WB, Liu JH, Wang H. 2019. Spatio-temporal patterns of drought evolution over the Beijing-Tianjin-Hebei region. J Geogr Sci. 29(6):863–876.

Zhang XX, Zhang Y, Xu HJ. 2015. Regularity analysis of hydro-meteorological elements in the upper reaches of the Bailong River. J Arid Land Res Environ. 29(2):172–178.

Zhou LT. 2009. Inter-annual variability of summer rainfall in North China. J Atmos Sci. 32 (3):412–423.

Zhou D, Zhang B, Luo J, Zhang CL, An ML, Wang D. 2014. Basic of SPEI characteristics and genetic analysis of occurrence intensity of drought in North China in recent 500 years. J Nat Disaster. 23 (4):192–202.

Zhu NH, Bai XM, Dong WJ. 2013. Harmonic detection method based on EEMD. Pro CSEE. 33(7):92–98.

Zou YL. 1995. Transition of north agriculture pastoral transitional zone and changes of climate cold and warm in the Ming and Qing Dynasties. J Fudan Univ. (1):26–33.

Zou X, Zhai P, Zhang Q. 2005. Variations in droughts over China: 1951–2003. Geophys. Res. Let. 32:L04707.

Zuo DP, Cai SY, Xu ZX, Li FL, Sun WC, Yang XJ, Kan GY, Liu P. 2018. Spatiotemporal patterns of drought at various time scales in Shandong Province of Eastern China. Theor Appl Climatol. 131(1-2):271–284.